Article

Effects of Lateral Flows on the Supercavitation and Hydrodynamic Characteristics of Underwater Series and Parallel High-Speed Projectiles

Lite Zhang [ID]**, Chengwei Zhang, Huixia Jia ***[ID]** and Ruoling Dong**

National-Provincial Joint Engineering Laboratory for Fluid Transmission System Technology, Zhejiang Sci-Tech University, Hangzhou 310018, China
* Correspondence: huixia.jia@zstu.edu.cn

Abstract: In this paper, the supercavitation of the parallel and tandem projectiles moving underwater with high-speed under the condition with/without lateral flows is numerically simulated by the volume of fraction (VOF) model. The motion of the projectiles was handled by the overlapping grid and six degrees of freedom (DOF) techniques. The supercavitation evolution and the hydrodynamic characteristics of the projectiles were analyzed for the parallel and tandem projectiles under different conditions. The results show that the cavity shape is symmetrical under the condition without lateral flows, but is no longer symmetrical under the conditions with lateral flows. The asymmetry of the cavity contour increases with the velocity of the lateral flow. For the parallel projectiles, the change trends of the axial velocity of projectile 1 and projectile 2 are nearly the same. The offset velocity of projectile 1 and projectile 2 increases with the increase in the velocity of the lateral flow. The deflection angle of projectile 1 decreases with the increase in the lateral flow velocity but that of projectile 2 increases with the increase in the lateral flow velocity. At t = 3.0 ms, the deflection angle of projectile 2 is up to 20° under the condition of the lateral flow velocity of 11.25%, while the deflection angle of projectile 1 and 2 under other conditions is in the range of 5°. For the tandem projectiles, the axial velocity of projectile 1 gradually decreases. The change trend of the axial velocity of projectile 2 at first is the same as that of projectile 1, and then the change is dependent on the velocity of the lateral flow. Under the condition of the lateral flow velocity with 11.25%V_p, projectile 2 cannot enter the cavity of the front projectile. The change trend of the axial velocity of projectile 2 is similar as but somewhat slower than that of projectile 1. For the parallel projectiles, the ballistic stability of the projectile on the oncoming side is better than that of the projectile on the backflow side. Whether parallel or tandem projectiles, the ballistic stability of projectile 2 becomes worse with the increase in the lateral flow velocity.

Keywords: supercavitation; lateral flow; parallel projectiles; tandem projectiles

1. Introduction

The pressure around an object moving underwater will decrease with the increase in its velocity. When the pressure is reduced to the local saturated steam pressure, cavitation will happen [1]. When the cavity wraps around the entire surface of the object, the so-called "supercavitation" is formed [2]. The drag reduction of the object wrapped by supercavitation can be more than 90% [3]. So, the supercavitation technology is extensively applied in the design of the underwater guns, underwater high-speed torpedoes, anti-submarine rockets, submarine-launched missiles and other weapons. With the development of supercavitation, the cavity will collapse accompanied with the release of a large amount of energy, which may cause mechanical damage to objects, but also can be utilized in some fields [4,5]. Therefore, it is important to understand the supercavitation mechanism.

In view of the supercavitation flow, researchers have carried out much theoretical and experimental research. Savchenko et al. [6,7] conducted a large number of experimental

studies on the supercavitation flow of high-speed underwater objects and improved the empirical formula of the supercavitation shapes with cavitation numbers in the range of 0.012 to 0.057.

Hrubes et al. [8] carried out the study of the cavity characteristics and ballistic stability of underwater projectiles with the speed of up to 1100 m/s. They found that the instantaneous impact caused by the collapse of the cavity is very huge, and can reach more than 200 times the gravitational acceleration.

Vlasenko et al. [9] experimentally analyzed the shape of the cavitation under subsonic and supersonic conditions, and obtained the influence of compressibility on the supercavitation flow. Nguyen et al. [10] numerically analyzed the characteristic parameters of supercavitation flow around supersonic and transonic projectiles.

In the experimental research of Shi and Takami [11] about the water-entry of a high-speed projectile, they found that the projectile trajectory deflects due to the strongly three-dimensional and chaotic characteristics of the flow field in water.

Truscott et al. [12] experimentally investigated the water-entry of rotating spheres under low Froude numbers. They found that the water splashing and the shape of the cavitation produced by rotating spheres changed significantly, compared with non-rotating spheres. The trajectory of spheres was also noticeably deflected. Later, Speirs et al. [13] experimentally conducted the study of the water-entry of spheres with different contact angles. They found that the cavity shapes are not only dependent on the Bond number and Weber number, but also on the contact angle.

Li et al. [14] numerically studied the effect of the initial velocity, rotation speed and attack angles of projectiles on the ballistic characteristics during the water-entry process. The results showed that the rotation speed of the projectile has little effect on the velocity of the projectile, but it affects the movement stability of the projectile.

Recently, Jia et al. [15] experimentally investigated the effects of surface coatings of a projectile on the supercavitation and hydrodynamics of projectiles. They found that the hydrophilicity or hydrophobicity of the surface significantly affects the supercavitation flow. At the same water depth and cavitation number, the size of the supercavitation of the projectile with hydrophobic coating is greater than that of the projectile with hydrophilic coating, and the drag force coefficient of the hydrophobic projectile is obviously smaller than that of the hydrophilic projectile.

In addition, many researchers have carried out studies regarding the effects of head shapes of projectiles on supercavitation [16,17].

The above studies focus on a single body. For parallel or series projectiles, the studies available are relatively few.

Lu et al. [18] experimentally investigated the effects of the spacing between two tandem projectiles on the interaction of the cavitation and trajectory of projectiles. They found that the effect on the trajectory due to the interaction of the cavity of two projectiles is significant. With the increase in the spacing, the pressure on the second projectile and projectile trajectory gradually approach those of the first projectile. Xu et al. [19] numerically simulated the flow field of two continuously launched projectiles and analyzed the interaction between the wake vortex and the projectile with different launch velocities and launch sequences. They found that the stability of the latter projectile is significantly affected by the wake vortex. Lu et al. [20] numerically studied the water-entry of asynchronously parallel projectiles. They found that the cavity of the asynchronously parallel projectiles is deformed because of the interaction of the two projectiles. The movement stability of the latter projectile is worse than that of the front one. Qi et al. [21] numerically simulated the supercavitation flow of two parallel projectiles. They found that the parallel projectiles are more easily wrapped by supercavitation than a single projectile. Zhou et al. [22] numerically simulated the water-entry and water-exit of two successively fired projectiles. They found that the second projectile can enter into the cavity of the first projectile.

All of the above studies were carried out in still water without considering the presence of lateral flow. The research considering the presence of lateral flow is relatively rare.

Yu et al. [23] numerically simulated the water-entry of synchronously parallel projectiles under conditions with lateral flow. They found that the head of the projectiles approach each other with a lower velocity of the lateral flow, while the head of the projectiles separate from each other with a higher velocity of the lateral flow.

Wang et al. [24] numerically analyzed the influence of the lateral flow velocity on the supercavitation using OPENFoam. They found that the higher the convection velocity, the weaker the influence of the lateral flow on the cavity profile and drag force under the same lateral velocity.

In the above studies considering the effect of the lateral flow, it should be pointed out that the change in the velocity and the trajectory of the projectile was not considered; that is, the projectile is fixed in the studies, which is unreasonable to address the real problem.

In this study, the cavitation flow of tandem projectiles and parallel projectiles under different lateral flow conditions are numerically simulated. The attenuation of projectile velocity and the deflection of ballistic trajectory of the parallel and tandem projectiles was considered using the six degrees of freedom (6DOF) technology. The effect of the lateral flow on the cavitation and kinematic characteristics of the projectiles are analyzed and discussed.

2. Theoretical Model and Numerical Methods

The flow is a two-phase flow when a projectile moves underwater with high speeds considering the cavitation of the water. In tise paper, the volume of fraction (VOF) model was used to solve the two-phase flow field. The continuity and momentum equations of the mixed-phase are given in Equations (1) and (2), respectively.

$$\frac{\partial \rho}{\partial t} + \frac{\partial (\rho u_i)}{\partial x_i} = 0 \tag{1}$$

$$\frac{\partial (\rho u_i)}{\partial t} + \frac{\partial (\rho u_i u_j)}{\partial x_i} = -\frac{\partial P}{\partial x_j} + \frac{\partial \tau_{ij}}{\partial x_i} + S_M \tag{2}$$

where ρ is the density of mixed phase (kg/m^3); t is the time (s); u_i is the velocity component of the mixed phase in the i-direction (m/s); P is the pressure (Pa); τ_{ij} is the viscous shear stress (N/m^2) and is given by Equation (3).

$$\tau_{ij} = \mu \left[\left(\frac{\partial u_i}{\partial x_j} + \frac{\partial u_j}{\partial x_i} \right) - \frac{2}{3} \delta_{ij} \frac{\partial u_l}{\partial x_l} \right] \tag{3}$$

where μ is the dynamic viscosity of the mixed phase (Pa·s), δ_{ij} is the Kroneker symbol (-); S_M is an additional source term (Pa/m). The expressions of ρ and μ are given in Equations (4) and (5), respectively.

$$\rho = \alpha_v \rho_v + (1 - \alpha_v) \rho_l \tag{4}$$

$$\mu = \alpha_v \mu_v + (1 - \alpha_v) \mu_l \tag{5}$$

where α_v is the volume fraction of water vapor phase (-); ρ_l and ρ_v are the density of water and water vapor, respectively; μ_l and μ_v are the dynamic viscosity of water and water vapor, respectively.

In this paper, the RNG κ-ε turbulence model [25] was used to simulate the turbulent flow field. The governing equations of turbulent kinetic energy κ and dissipation rate ε are given in Equations (6) and (7), respectively.

$$\frac{\partial (\rho k)}{\partial t} + \frac{\partial (\rho k u_i)}{\partial x_i} = \frac{\partial}{\partial x_j} \left(\alpha_k \mu_{eff} \frac{\partial k}{\partial x_j} \right) + G_k - \rho \varepsilon \tag{6}$$

$$\frac{\partial(\rho\varepsilon)}{\partial t} + \frac{\partial(\rho\varepsilon u_i)}{\partial x_i} = \frac{\partial}{\partial x_i}\left(\alpha_\varepsilon \mu_{eff}\frac{\partial\varepsilon}{\partial x_j}\right) + C_{1\varepsilon}\frac{\varepsilon}{k}G_k - C_{2\varepsilon}\rho\frac{\varepsilon^2}{k} \tag{7}$$

where κ is the turbulent kinetic energy (m^2/s^2); ε is the dissipation rate (m^2/s^3); $\mu_{eff} = \mu + \mu_t$, μ_t is turbulence viscosity; α_κ, α_ε are the Prandtl numbers of negative effects of κ and ε, respectively; G_k is the generation term of the turbulent kinetic energy induced by the velocity gradient; $C_{1\varepsilon}$, $C_{2\varepsilon}$ are the empirical constant of turbulence kinetic energy and dissipation rate, respectively.

The Schnerr–Sauer cavitation model [26] was adopted to consider water cavitation. The general form of its equation is given in Equation (8).

$$\frac{\partial}{\partial t}(\alpha_V\rho_V) + \nabla\cdot(\alpha_V\rho_V v_V) = R_e - R_c \tag{8}$$

where R_e and R_c are the evaporation and condensation rate (kg/(m^3·s)), respectively, and given in Equations (9) and (10), respectively.

$$R_e = \frac{\rho_V\rho_1}{\rho}\alpha_v(1-\alpha_v)\frac{3}{r_B}\sqrt{\frac{2}{3}\left(\frac{P_V - P}{\rho_1}\right)},\ P_V > P \tag{9}$$

$$R_c = \frac{\rho_V\rho_1}{\rho}\alpha_v(1-\alpha_v)\frac{3}{r_B}\sqrt{\frac{2}{3}\left(\frac{P - P_V}{\rho_1}\right)},\ P_V < P \tag{10}$$

where r_B is the radius of the gas core (m); P_v is the saturated vapor pressure of water (Pa). In all of the above equations, the international unit for each physical parameter is used.

The physical model of the projectile is shown in Figure 1, which is a cylinder with the length L = 36 mm and diameter D = 6 mm. The ratio of the length to the diameter is 6.
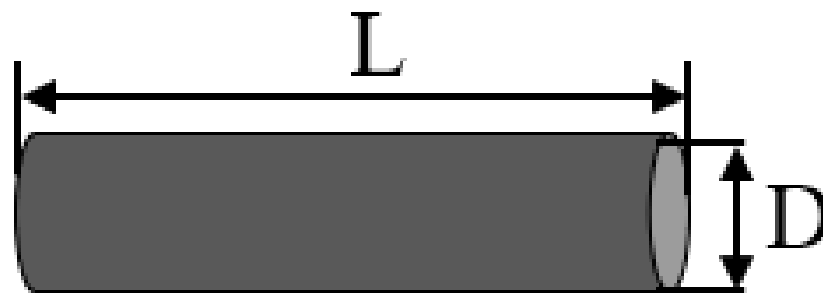

Figure 1. Physical model of the projectile.

Figures 2 and 3 show the computational domain and boundary conditions of the numerical simulation for the parallel and tandem projectiles in the environment with lateral flows, respectively. The computational domain is a rectangular area of $90D \times 25D \times 25D$, seen in Figures 2a and 3a. The size of the domain is enough to avoid boundary effects and satisfies the requirement of the free movement of projectiles. As shown in Figures 2b and 3b, the lower boundary condition is set as the velocity inlet, the surface of the projectile is set as no-slip wall, and the other boundary conditions are the pressure outlet. The spacing between two parallel projectiles is $\Delta Hp = D$; the spacing between two tandem projectiles is $\Delta Hc = 6D$. The initial velocity of the projectile is along the x-axis and the lateral inflow is along the z-axis.
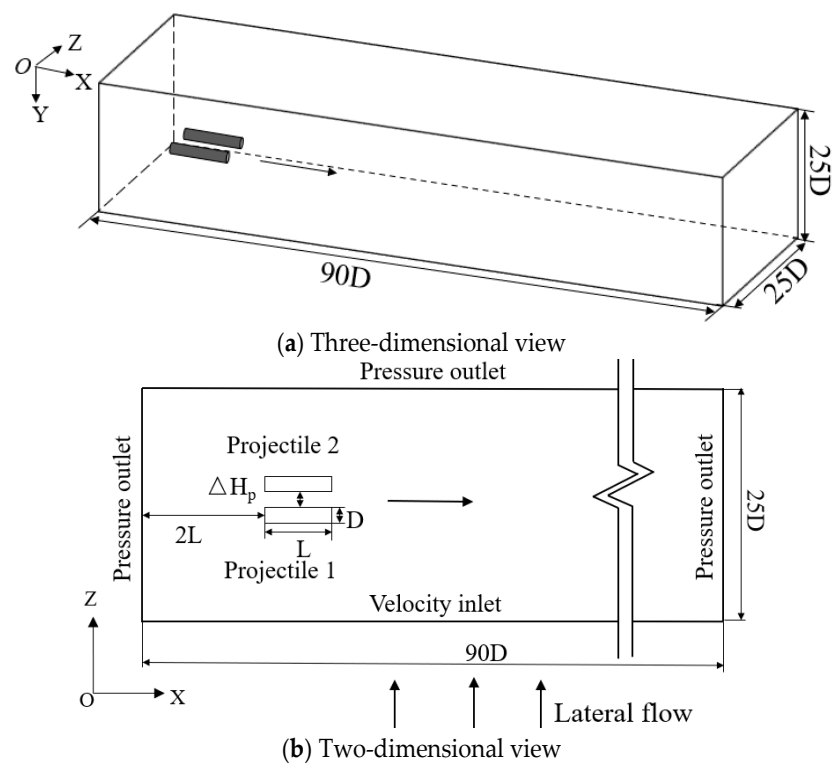
Figure 2. Schematic diagram of the computational domain and boundary conditions of the parallel projectiles.
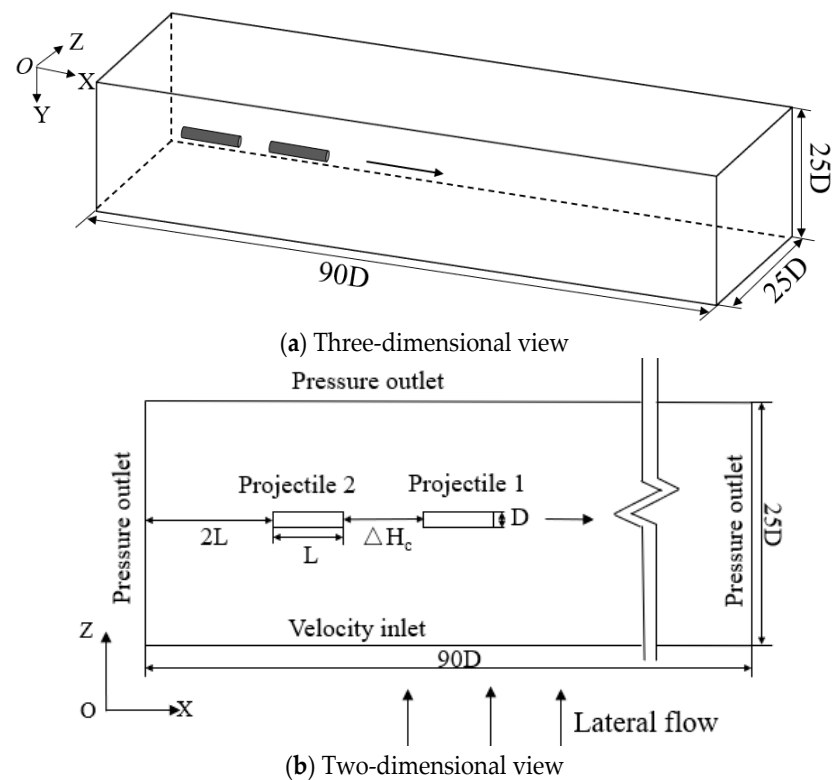

Figure 3. Schematic diagram of the computational domain and boundary conditions of the tandem projectiles.

The 2-dimensional view (in xoy plane) of the used 3-dimensional meshes for the simulation of underwater movement of the parallel and series projectiles is given in Figure 4.

In the whole domain structured grids were adopted, and around the projectile the mesh was densified. The maximal distance between the first grid point and the projectile wall is about 3×10^{-6} m and the $y+$ satisfies the requirement of solving the viscous sublayer. The motion of the projectile is handled by overlapping meshes and six degrees of freedom (DOF) techniques. For the overlapping meshes, the background grid covers the entire computational domain and the component grid is around every projectile. For the 6DOF technique, the physical parameters of the translational motion of the projectile are obtained by solving Equation (11) in the inertial coordinate system.

$$m\frac{d\vec{V}_G}{dt} = \vec{F}_G \tag{11}$$

where m is the mass of the projectile, $\vec{V}_G$ is the velocity vector of the center of mass of the projectile and $\vec{F}_G$ is the force vector on the center of mass of the projectile. The angular motion of the projectile is solved by Equation (12) in the body coordinate system.

$$\frac{d\vec{\omega}_B}{dt} = \boldsymbol{L}^{-1}\cdot\left(\sum \vec{M}_B - \vec{\omega}_B \times (\boldsymbol{L}\cdot\vec{\omega}_B)\right) \tag{12}$$

where $\boldsymbol{L}$ is the inertia tensor, $\vec{\omega}_B$ is the angular velocity vector of the projectile and $\vec{M}_B$ is the moment vector acting on the projectile.
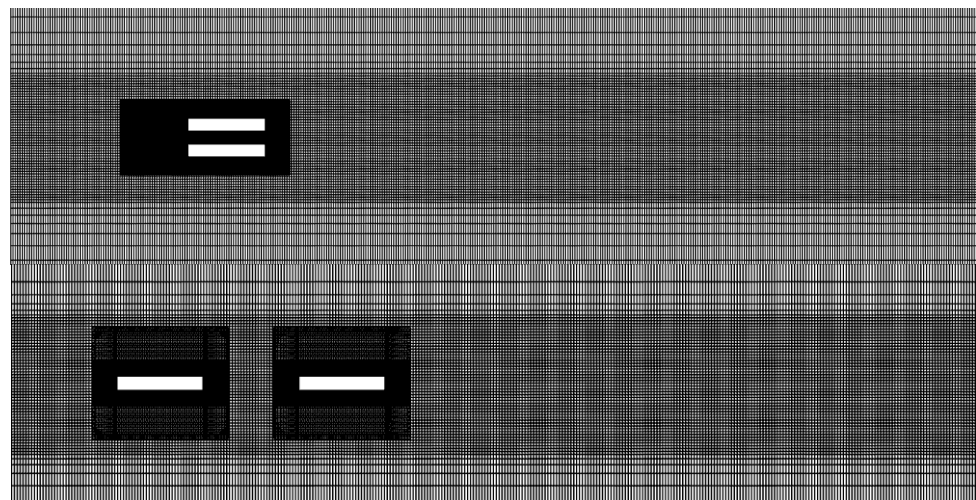

Figure 4. Schematic diagram of the two-dimensional grid in the xoy plane.

In the numerical simulation, the pressure–velocity fields are solved by coupled algorithm, The space discretization of the pressure field adopts the PRESTO! scheme. The Modified HRIC scheme was used to handle the interface of phases. In the simulation the used time step is 1×10^{-6} s.

3. Verification of Grid Independence and Numerical Methods

In the numerical simulations of this paper, the grid-independence verification was first performed. In total, 3 sets of grids with different densities (case1, case2, case3) are established for the simulation of a single projectile, and the number of grids is 0.6 million (case1), 1.4 million (case2) and 1.8 million (case3), respectively. Figure 5 shows the comparison of the velocity variation of the projectile for cases 1–3. It can be seen from the figure that the difference between case 1 and case 2 is somewhat obvious in the locally enlarged diagram, but the difference between case 2 and case 3 can be neglected even in the locally enlarged diagram. Considering the calculation accuracy and computational efficiency, the same grid topology and grid density as in case 2 are used in the later numerical simulations.
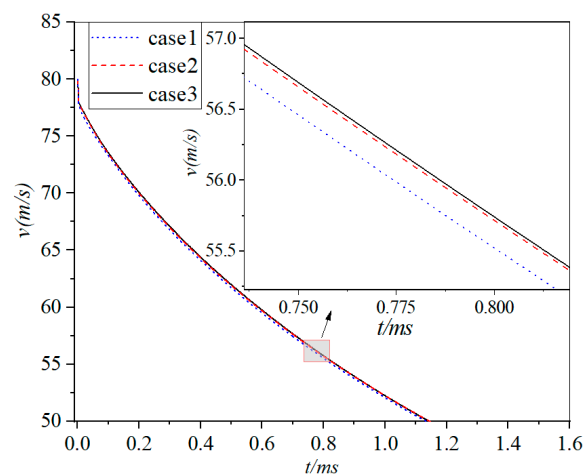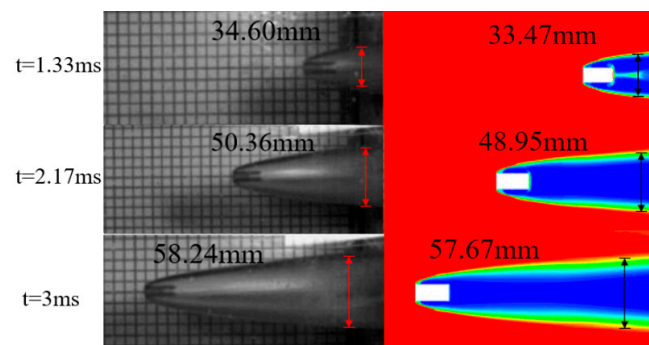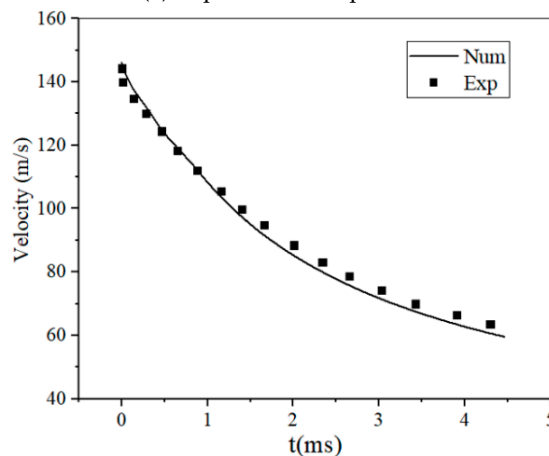
Figure 5. Comparison of velocity change in the projectile for three cases with different grid numbers.

On the basis of the mesh-independence verification, the simulation results were compared with the experimental data. [16] The parameters of the geometry and initial motion of the projectile in the numerical simulation is the same with that in the experiment. The diameter and length of the cylinder is 12.66 mm and 25.4 mm, respectively, and the initial velocity of the projectile is 146 m/s. Figure 6a shows the comparison of the profile of the supercavitation at different times between the experimental data and numerical results. It can be seen that the numerical results and the experimental data agree well and the maximum error is about 3.2%. Figure 6b,c shows the comparison of the change in the velocity and displacement along the initial direction of the projectile between the simulation results and experimental data, respectively. Similarly, it can be seen that the agreement between the simulation results and the experimental data are good.
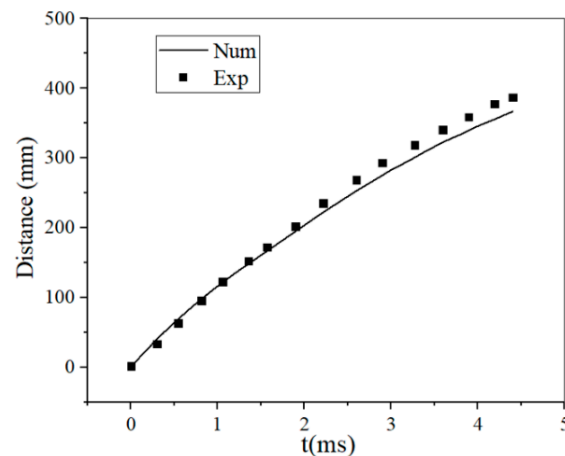

(**a**) Supercavitation profile

(**b**) Velocity change in the projectile with time

Figure 6. *Cont*.

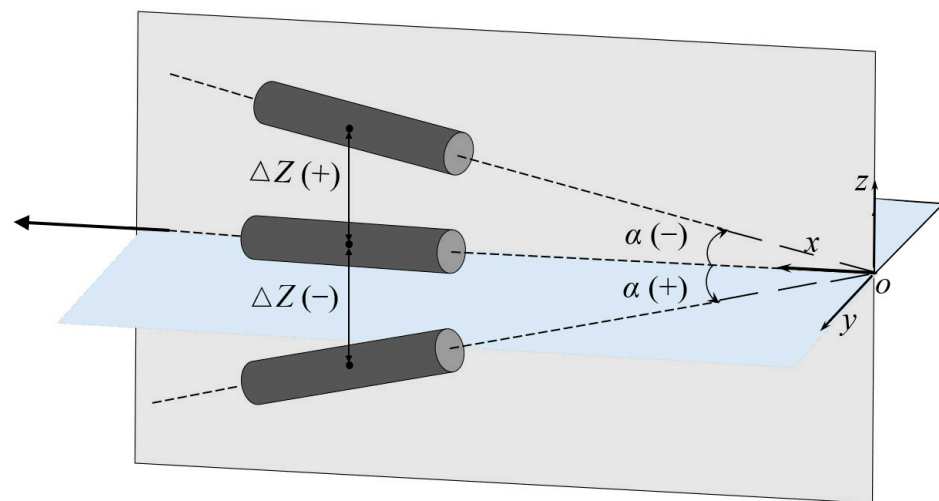(**c**) Displacement change in the projectile with time

Figure 6. Comparison between simulation results and experimental data [16].

4. Results and Discussions

4.1. Supercavitation Flow of Parallel Projectiles under the Effect of Lateral Flow

In this section, the supercavitation flow field of two parallel projectiles was simulated under different conditions with and without lateral flow. The spacing ΔH_p between the two parallel projectiles is the same as the diameter D of the projectile. The initial velocity of both projectiles is V_p = 80 m/s, which is along the x-axis. The lateral flow direction is perpendicular to the direction of the initial velocity of the projectile and along the z-axis. The 3 investigated velocities V_c of the lateral flow are 3.75%V_p, 7.5%V_p and 11.25%V_p, respectively.

For the convenience of the following discussion, it is necessary to clearly give some definitions of the physical parameters later discussed. Figure 7 shows the schematic diagram of the kinematic parameters of projectiles, and the direction of the lateral flow is also shown in the figure. The direction of the initial velocity of the projectile is along the x-direction, and the lateral flow is along the z-direction. In the following section, the velocity component of the projectile in the x-direction is named axial velocity, and the component in the z-direction is called offset velocity. Correspondingly, the displacement in the z-direction is defined as offset displacement.

Figure 7. Schematic diagram of the definition of the kinematic parameters of a projectile.

According to the obtained numerical results, the velocity component in the y-direction of the projectile is much smaller than that in the z-direction and can be ignored. Thus, it can be considered that the projectile moves in the xoz plane and deflects only around the

y-axis. The definitions of the deflection angle α around the y-axis and the displacement of the projectiles in the z-direction are also shown in Figure 7. It is specified that the deflection angle α is positive with a counterclockwise rotation around the y-axis, and vice versa. The offset displacement along the positive z-axis is positive, and vice versa. In addition, it should be remembered that the velocity component in the y-direction and the deflection angle around the x- or z-axis of the projectile are very small and can be neglected; they will no longer be given and discussed later.

In order to clearly explain the meaning of the terms used later, Figure 8 gives the schematic diagram of the definition of different zones in the flow field. When the projectiles move along the x-axis perpendicular to the lateral flow, the zone on one side of the projectile firstly affected by the lateral flow is defined as the oncoming side and the other side is called the outflow side. For the two parallel projectiles, the zone between the two projectiles is named the inner side or inside zone, while the other zone is defined as the outer side or outside zone. It should be noticed that the inside zone between the two parallel projectiles is the backflow side of projectile 1, but is the oncoming side of projectile 2.
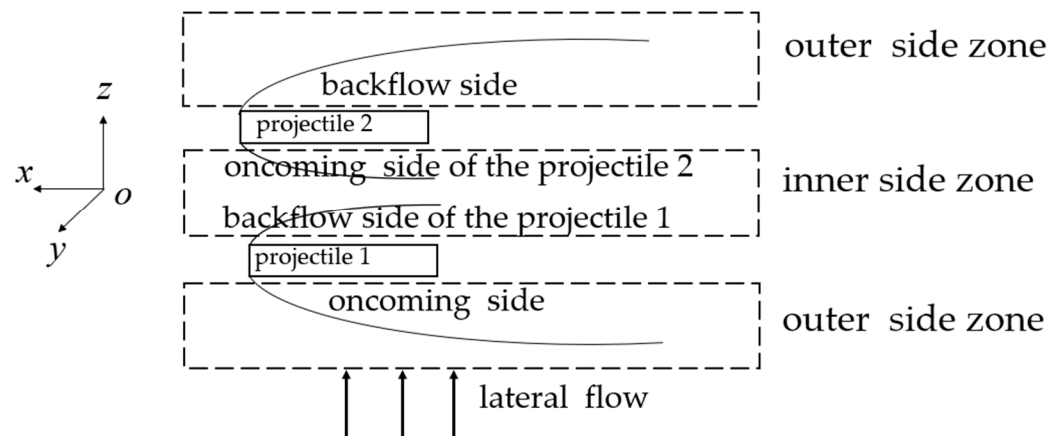

Figure 8. Schematic diagram of the definition of different zones in the flow field.

When two projectiles move in parallel, the projectile which is first affected by the lateral flow, is defined as projectile 1 and the other is named projectile 2. Figure 9 shows the water phase diagram of the supercavitation flow field of the parallel projectiles under different conditions. Figure 9a shows the cavity evolution around the two parallel projectiles without lateral flow. It can be seen from Figure 9a that at $t = 0.2$ ms the cavities firstly appear at the shoulders and tail of the projectile. The shoulder cavity around every projectile is not symmetrical, and the size of the cavity in the inside zone between the two projectiles is smaller than that in the outside zone, which may be caused by the higher pressure in the zone between the two projectiles. At $t = 0.8$ ms, the cavity size gradually increases and tends to form a supercavity, but at this time, the cavity size in the inside zone is still obviously smaller than that in the outside zone. At this time, it is also observed that the direction of the movement of the two projectiles is symmetrically changed. At $t = 1.4$ ms, the 2 cavities at the tail of the 2 projectiles are fused into 1 cavity and the size of the cavity continues to increase. The trajectories of the two projectiles continue to symmetrically deflect. At $t = 2$ ms, the size of the cavity increases continuously. In addition, if the two projectiles are viewed as a whole and named the parallel projectile group, under the condition without lateral flow the cavitation around the parallel projectile group seems to be symmetrical, and the trajectory change in the two projectiles also seems to be symmetrical. The heads of both projectiles are deflected by a tendency to separate from each other.
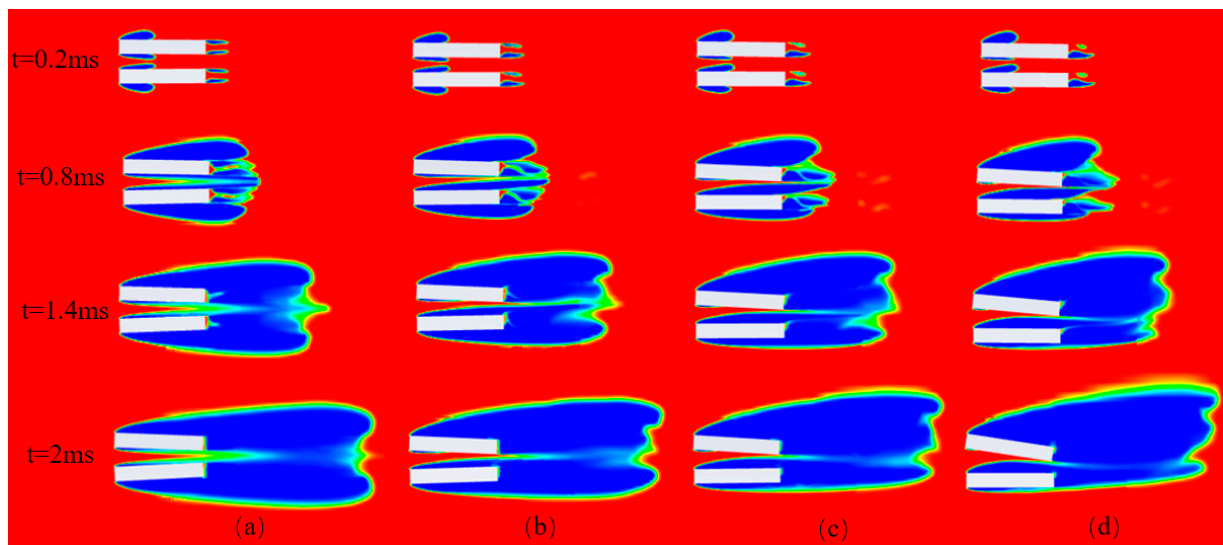
Figure 9. Evolution of the cavitation of parallel projectiles at different conditions: (**a**) no lateral flow; (**b**) the lateral flow velocity $V_c = 3.75\%V_p$; (**c**) $V_c = 7.5\%V_p$; (**d**) $V_c = 11.25\%V_p$.

Figure 9b shows the cavity evolution under the condition of the lateral flow velocity with $3.75\%V_p$. It can be observed that the symmetry of the cavitation profile of the parallel projectile group disappears under the condition with a lateral flow.

Even at $t = 0.2$ ms, it can be observed that the size of the cavity of projectile 1 is bigger than that of projectile 2 in the inside zone, while in the outside zone the size of the cavity of projectile 1 is smaller than that of projectile 2. The reason may be as follows: on one hand, under the effect of the lateral flow, the size of the cavity on the oncoming side is decreased and that on the backflow side is increased; on the other hand, the higher pressure between the two parallel projectiles suppresses the growth of the cavity on the inside zone.

At $t = 0.8$ ms, it can be observed that the cavity profile on the oncoming side of projectile 2 is thinner than that under the condition with no lateral flow. At $t = 1.4$ ms, the cavity profile on the oncoming side of projectile 2 becomes thinner, so that the rewetted zone appears at the tail of the projectiles. In addition, the fusion process of the cavity at the tail under this condition has not been completed (Figure 9b), while under the condition without lateral flows, this process is already completed at this time.

Comparing Figure 9b–d, it can be seen that with the velocity increase in the lateral flow, the thickness of the cavity on the oncoming side of projectile 1 and 2 decreases, while the thickness of the cavity on the backflow side increases. Because the oncoming side of projectile 2 is located in the inside zone between the two projectiles, the size of the cavity on the oncoming side of projectile 2 is smaller than that of projectile 1 under the same condition. Thus, the rewetted zone easily appears on the oncoming side of projectile 2. Furthermore, the rewetted zone increases with the increase in the lateral flow velocity.

At $t = 0.8$ ms, under the condition without lateral flow, the wall of projectile 2 has been completely covered by the cavity; under the condition of the lateral flow velocity with $3.75\%V_p$, the cavity size on the oncoming side of projectile 2 obviously decreases and tends to disappear at the tail. Under the condition of the lateral flow velocity with $7.5\%Vp$, the wall on the oncoming side at the tail of projectile 2 is rewetted; under the condition of the lateral flow velocity with $11.25\%Vp$, the rewetted zone increases. It can be also seen from Figure 9 that the deflection of the trajectory of projectile 2 become bigger with the increase in the velocity of the lateral flow, while the deflection of projectile 1 seems to be smaller.

Figure 10 shows the cavity contour at a cross section parallel with the yoz plane at $t = 1.4$ ms for different conditions. The cross-section is located at 25% from the head of the projectile. It can be seen that the cavity contour is symmetrical in the y-direction for all conditions, but is asymmetrical in the z-direction. The asymmetry of the cavity contour

increases with the velocity of the lateral flow. Furthermore, it can be easily seen that the asymmetry of the cavity contour for projectile 2 is more obvious than that for projectile 1.
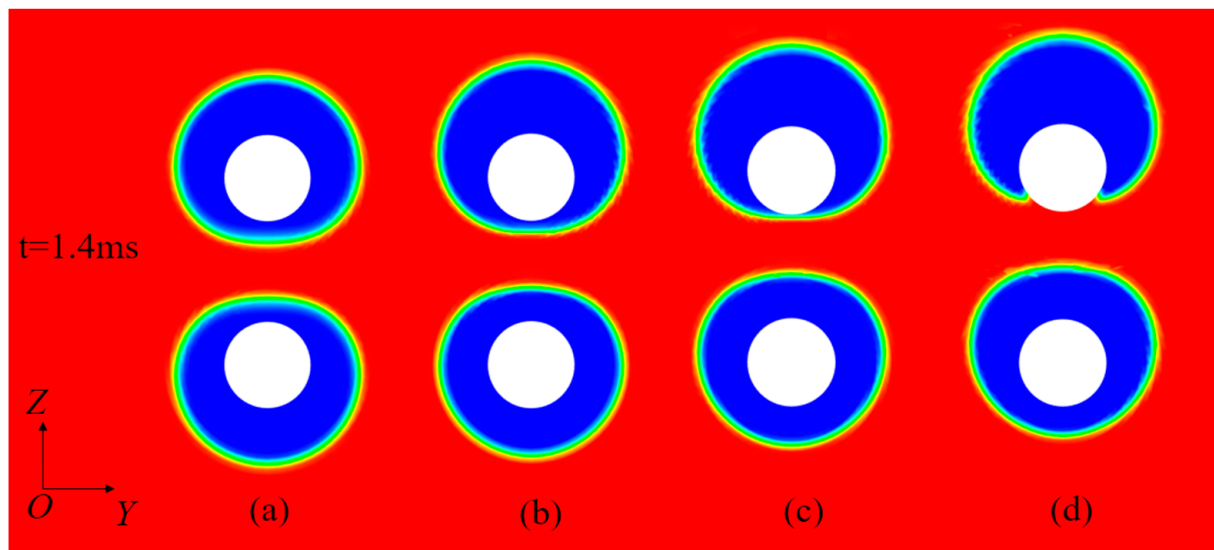

Figure 10. Cavity contour at a cross section parallel with the yoz plane (25% from the head of the projectile) under different conditions: (**a**) no lateral flow; (**b**) the lateral flow velocity $V_c = 3.75\% V_p$; (**c**) $V_c = 7.5\% V_p$; (**d**) $V_c = 11.25\% V_p$.

Figure 11 shows the comparison of the cavitation profiles of 2 projectiles at $t = 2$ ms under different conditions. The abscissa and ordinate are the dimensionless length L_c/D and diameter D_c/D of the cavity, respectively. It can be seen from the figure that the cavity around the projectile group is symmetrical under the condition without lateral flow, and for every projectile in the projectile group, the size of the cavity on the outer side of the projectile group is larger than that on the inner side. In the presence of the lateral flow, the cavity contour of the projectile group is no longer symmetrical. Furthermore, with the increase in the lateral flow velocity, the cavity size of projectile 1 on the inner side increases while the size on the outer side decreases. The change in the cavity size of projectile 2 is opposite to that of projectile 1; the size on the inner side decreases while it increases on the outer side.
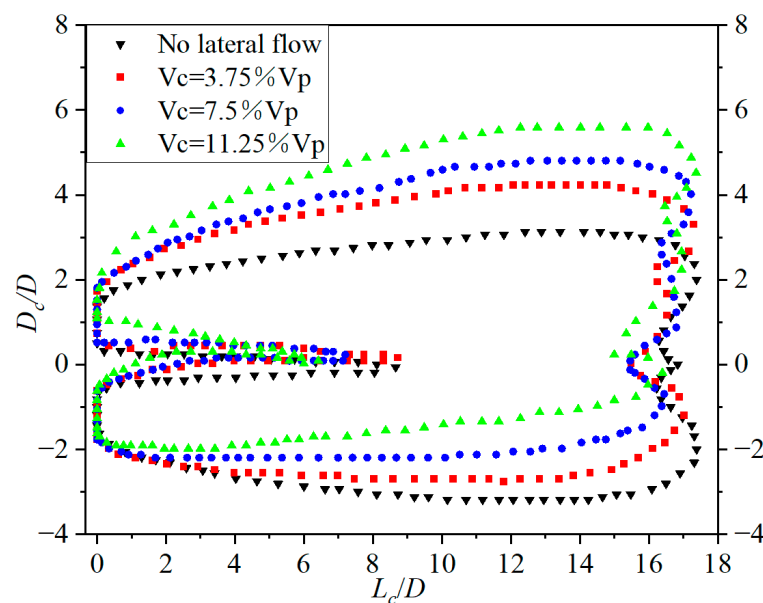

Figure 11. Comparison of the cavitation contours at $t = 2$ ms.

Figure 12a,b shows the pressure and velocity contours around the projectile group under the condition of the lateral flow velocity with $V_c = 7.5\% V_p$ at $t = 2$ ms. It can be seen from Figure 12a that the pressure near the head of projectiles is higher and that near the tail is lower. Near the head of projectile 2, the pressure distribution of the inner and outer sides is asymmetrical, and the inner side pressure is slightly higher than that of the outer side, which makes projectile 2 deflect clockwise, which can also be seen in the subsequent results of the deflection angle of the projectiles. In addition, it can be seen that in the middle zone between two projectiles the pressure near the projectile head is higher than that near the projectile tail. For this reason, the heads of the two projectiles deflect from each other. In Figure 12b, it can be seen that near the projectiles, the velocity on the backflow side is somewhat greater than that on the oncoming side due to the effect of the lateral flow. Additionally, the velocity on the backflow side of projectile 2 is slightly greater than that of projectile 1.
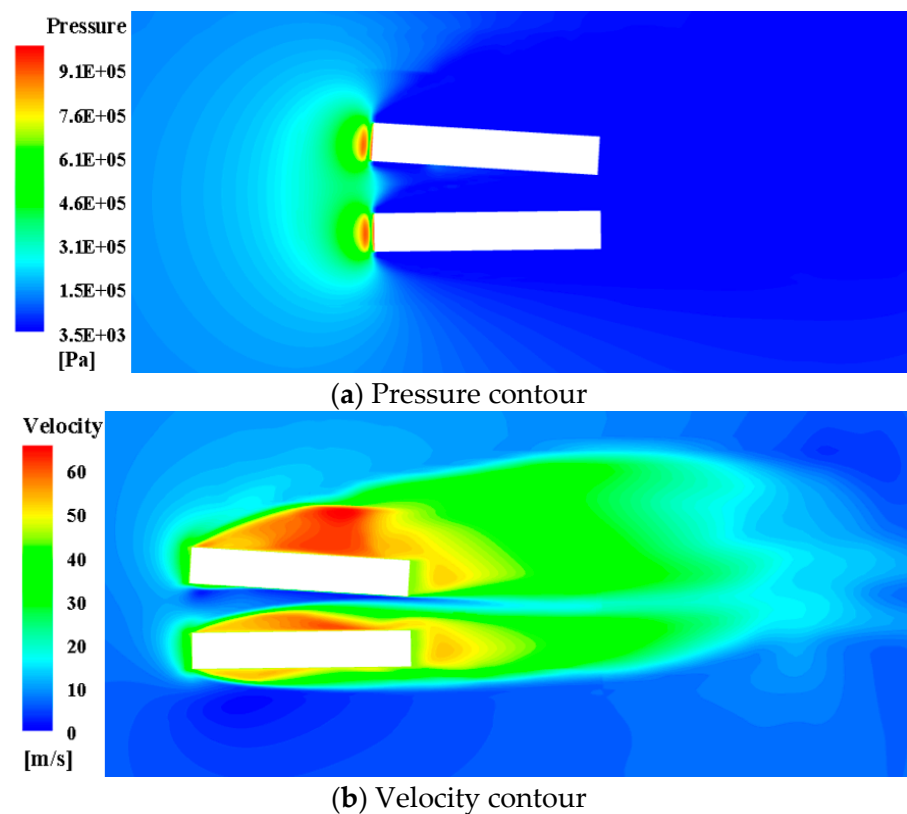

(**a**) Pressure contour

(**b**) Velocity contour

Figure 12. Pressure and velocity contours around the projectiles under the condition of the lateral flow velocity with *Vc* = 7.5%*Vp* (*t* = 2 ms).

Figure 13 shows the change in the axial velocity of two parallel projectiles under different conditions. The ordinate was nondimensionalized by the initial velocity V_p of the projectile. It can be seen from the figure that for different conditions the change trend of the axial velocity of the projectiles is nearly the same. From the locally enlarged diagram, it can be seen that the change in the axial velocity under conditions with lateral flow are faster than that under the condition without lateral flow. The reduction of the axial velocity becomes somewhat faster with the increase in the velocity of the lateral flow. In addition, the reduction in the velocity of projectile 2 is slightly faster than that of projectile 1 under the same condition, which may be due to the rewetted wall on the inner side of projectile 2.
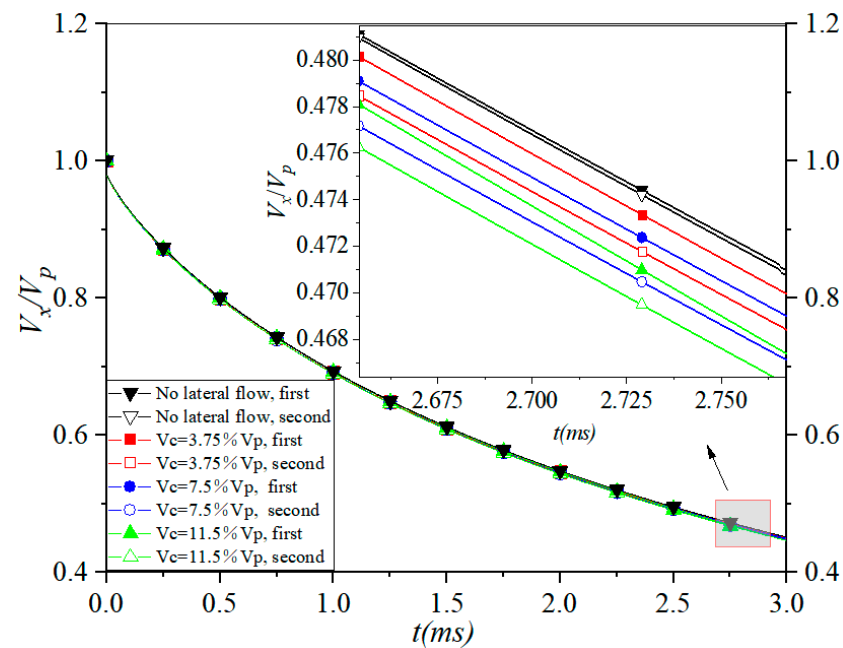
Figure 13. The change in the axial velocity of the parallel projectiles under different conditions.

Figures 14 and 15 show the change in the offset velocity and displacement of the two parallel projectiles in the z-direction under different conditions. The displacement of the ordinate in Figure 15 is nondimensionalized using the projectile diameter *D*.
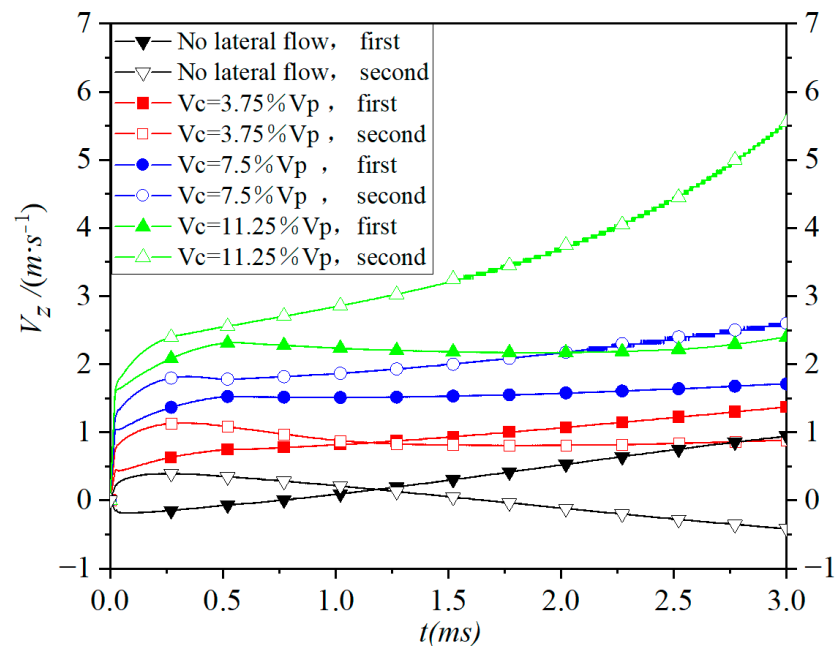

Figure 14. The change in the offset velocity of the projectiles in the z-direction.
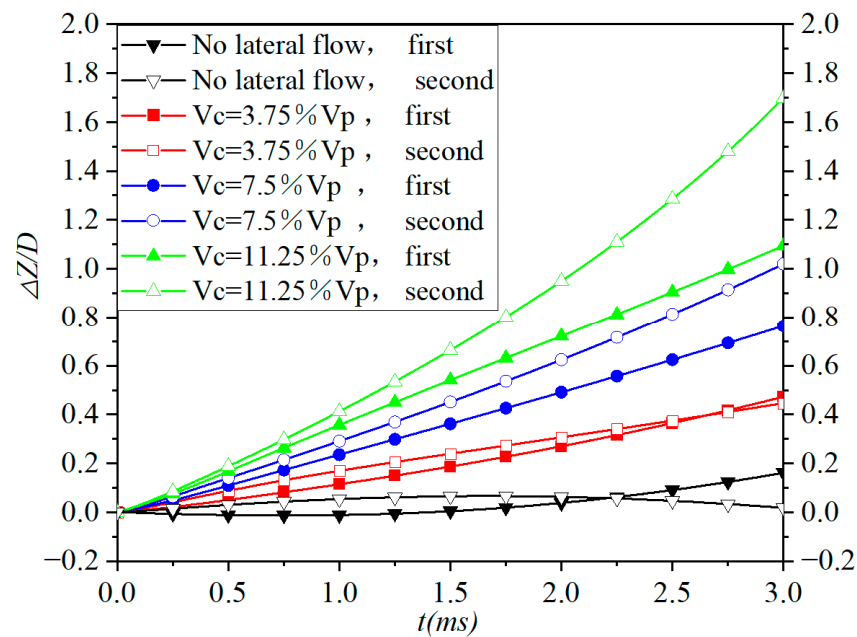
Figure 15. The change in the displacement of the projectiles in the z-direction.

It can be seen from Figure 14 that in the case of no lateral flow the offset velocity of projectile 1 and 2 is relatively small and in the range of 1 m/s, which can also be verified in the change in the displacement. At $t = 3.0$ ms, the change in the displacement of projectile 1 is less than $0.2D$. In addition, it can be seen from Figures 14 and 15 that the offset velocity and displacement are somewhat asymmetric for the case of no lateral flow, which may be induced by the unsteady and turbulent flow. In the numerical research of Watanabe et al. [27], they found that the forces on the projectile in air are asymmetric due to the unsteady vortices at the wake region of the projectile. The research of Shi and Takami [11] shows that the flow in water is more complex. They found that the motion of a high-speed underwater body is strongly three-dimensional and chaotic and the projectile trajectory will deflect due to the strongly three-dimensional and chaotic characteristics of the flow field.

Under the conditions with lateral flows, the offset velocities for both projectiles increase with the increase in the velocity of the lateral flow.

Under the condition of the lateral flow velocity with $3.75\% V_p$, the offset velocity of projectile 2 is slightly higher than that of projectile 1 at first, and then slightly lower than that of projectile 1 later. Additionally, the lateral spacing between the two projectiles remains nearly the same (Figure 15). When the lateral flow velocity is $7.5\% V_p$, the offset velocity of projectile 2 is higher than that of projectile 1. The spacing between the two projectiles increases (Figure 15). Furthermore, the offset velocity of projectile 2 gradually and slowly increases, while the offset velocity of projectile 1 remains nearly unchanged. For the conditions of $3.75\% V_p$ and $7.5\% V_p$, the offset velocity of the 2 projectiles at $t = 3.0$ ms is 30–40% of the lateral flow velocity.

When the velocity of the lateral flow is increased to $11.25\% V_p$, the difference in the offset velocity between the two projectiles increases. The offset velocity of projectile 2 is higher than that of projectile 1, and the rate of the change in the offset velocity of projectile 2 rapidly increases. At $t = 3.0$ ms, the offset velocity of projectile 1 is about 22% of the lateral flow velocity, while the offset velocity of projectile 2 is already up to about 60% of the velocity of the lateral flow. This means that the ballistic stability of projectile 2 is worse than that of projectile 1. This may be due to the seriously rewetted wall on the inner side of projectile 2 at this condition. For projectile 2, the pressure on the inside rewetted wall is obviously higher than that on the outside wall wrapped by the cavity. The force

on projectile 2 in the z-direction is seriously asymmetrical. Thus, the offset velocity of projectile 2 increases.

The change in the deflection angle α around the y-axis in the xoz plane with the time for different conditions is given in Figure 16. It can be seen from the figure that under the condition without lateral flows projectile 1 deflects counterclockwise, while projectile 2 deflects clockwise. The deflection angle of both projectile 1 and 2 gradually increases with the time.
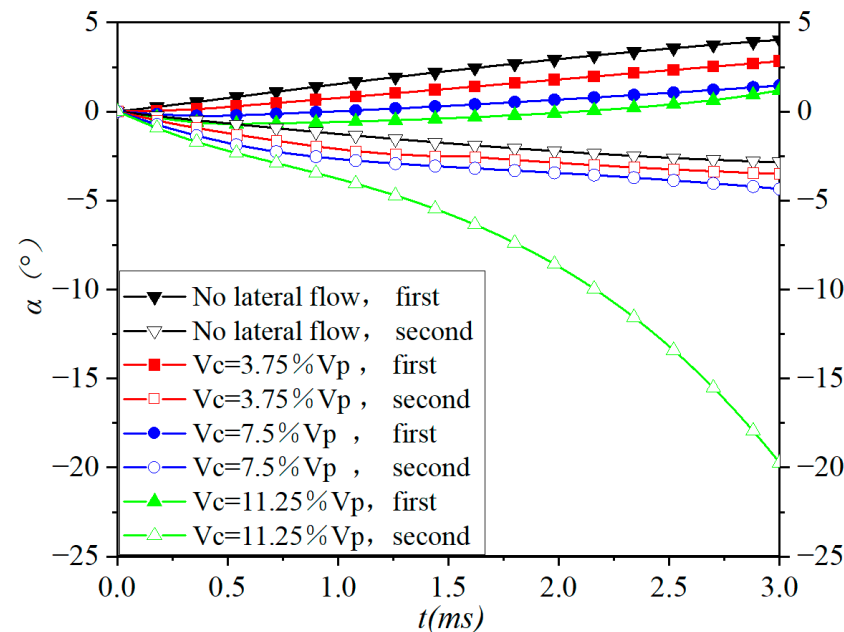

Figure 16. The change in the deflection angle α versus time.

Under the condition with lateral flows, the counterclockwise deflection angle of projectile 1 decreases with the increase in the velocity of the lateral flow, while the clockwise deflection angle of projectile 2 increases with the velocity increase in the lateral flow. The deflection angles of projectile 1 and 2 are within 5° under the condition with no lateral flow and the lateral flow velocity of $3.75\%V_p$ and $7.5\%V_p$ at $t = 3.0$ ms.

Under the condition of the velocity of the lateral flow at $11.25\%V_p$, the deflection angle of projectile 2 rapidly increases and can reach up to about 20° at $t = 3.0$ ms, while that of projectile 1 is only about 1°. This means the ballistic stability of projectile 1 is much better than that of projectile 2. In addition, the trajectory of projectile 2 significantly deviates from the initial one.

The decrease in the deflection angle of projectile 1 may be due to the fact that, for projectile 1, the effect of the high-pressure on the inner side of projectile 1 induced by the presence of projectile 2 and the action on the outside of projectile 1 induced by the lateral flow are canceled out by each other to some extent. For projectile 2, the oncoming side of the lateral flow is on the inner side of projectile 2. Then, the effect of the high pressure between two projectiles and the lateral flow are superimposed on the inner side of projectile 2. Thus, the deflection angle of projectile 2 increases with the increase in the lateral flow velocity.

4.2. Supercavitation Flow of the Tandem Projectiles in a Lateral Flow Environment

In this section, the supercavitation flow field of two tandem projectiles with different lateral flow velocities will be discussed. The spacing ΔH_c between the two tandem projectiles is 6D. The initial velocity V_p of the 2 projectiles is 80 m/s, which is the same as that used for the parallel projectiles. Additionally, the lateral flow velocities V_c are also the same as those used in the investigation of the parallel projectiles, which are $3.75\%V_p$, $7.5\%V_p$ and $11.25\%V_p$. Similarly with the study of the parallel projectiles, the motion of the tandem

projectiles is considered in the xoz plane and the velocity component in the y-direction is neglected due to the very small value. It is thought that the projectiles deflect only around the y-axis.

Figure 17 shows the 2-dimensional water phase diagram of the tandem projectiles moving underwater for different conditions in the xoz plane. Figure 17a shows the cavitation evolution under the condition without lateral flow. In the figure, the projectiles move from the right to the left.
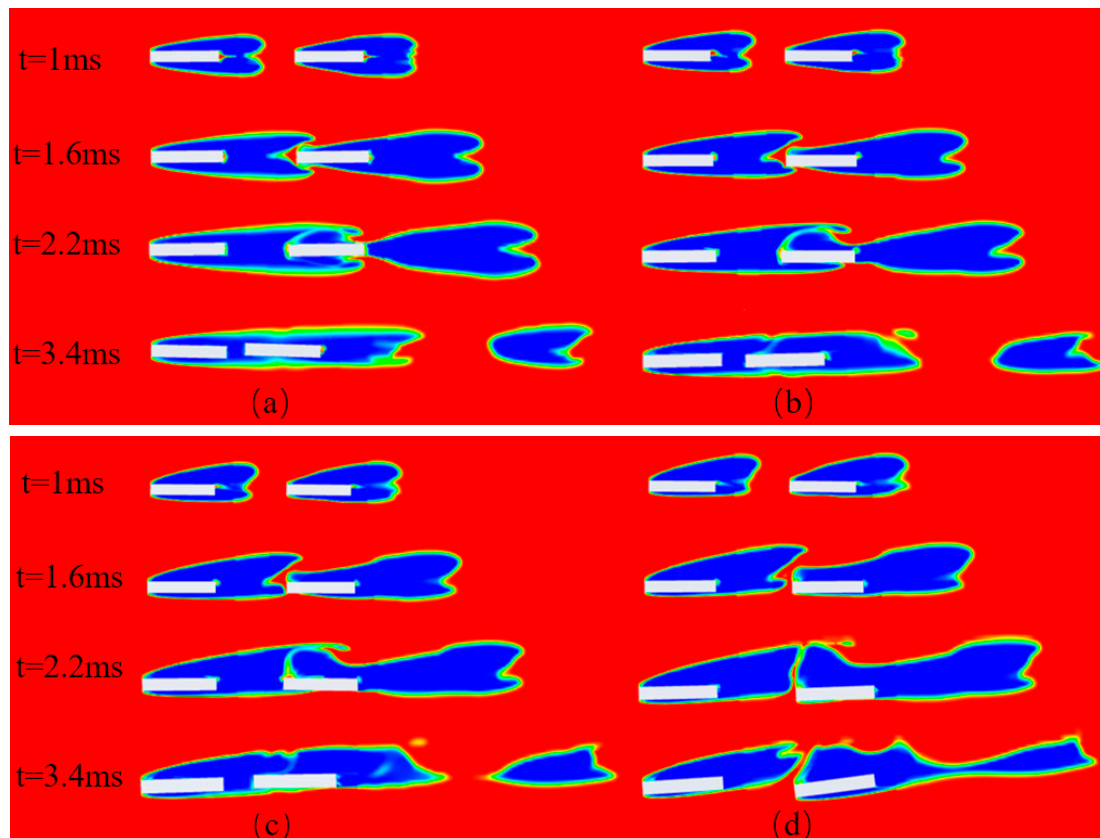

Figure 17. Cavity evolution of the tandem projectiles under different conditions: (**a**) no lateral flow; (**b**) the lateral flow velocity $V_c = 3.75\%V_p$; (**c**) $V_c = 7.5\%V_p$; (**d**) $V_c = 11.25\%V_p$.

It can be seen from Figure 17a both the first and second projectiles (also named projectile 1 and 2) have been wrapped by the cavity at $t = 1$ ms. Furthermore, the shape of the cavity is basically symmetrical along the axis of the projectile. The length of the cavity of both projectiles is nearly the same. At $t = 1.6$ ms, the head of the second projectile comes into contact with the tail of the cavity of the first projectile. At this time, the cavity profile near the head of the second projectile becomes thinner because of the extrusion of the tail cavity of the first projectile. At $t = 2.2$ ms, the head of the second projectile has entered into the cavity of the front projectile, and the cavity of the second projectile is extruded to the tail of itself by the influence of the cavity of the first projectile. At $t = 3.4$ ms, the second projectile has completely entered into the cavity of the front projectile. The distance between the two projectiles is decreased. This means that the speed of the second projectile may be greater than that of the first one, which can be verified in the following results regarding the velocity change. The cluster of the cavity falling off the second projectile will collapse under the action of the surrounding fluid.

Figure 17b shows the cavity evolution for the condition with the lateral flow velocity of $3.75\%V_p$. It can be observed from the figure that the symmetry of the cavity profile for the two projectiles no longer exists, which is due to the influence of the lateral flow. At $t = 1.0$ ms, it is already observed that the size of the cavity on the oncoming side of the

2 projectiles is smaller than that on the backflow side. At t = 2.2 ms the asymmetry of the cavity can be also obviously observed. On the oncoming side a part of the wall of the second projectile is still wetted, while on the backflow side the wall of the second projectile is completely wrapped by the cavity of the front projectile.

When the lateral flow velocity increases to 7.5%V_p, the asymmetry of the cavity profile is enhanced (Figure 17c). This asymmetry results in the increase in the wetted area on the oncoming side of the second projectile, compared Figure 17b,c at t = 2.2 ms or 3.4 ms. At t = 3.4 ms, the second projectile has entered the cavity of the first projectile, but there is still a wetted area at the tail of the second projectile on the oncoming side under this condition (Figure 17c). Under the condition without lateral flow and with the lateral flow velocity of 3.75%V_p, the second projectile is completely inside the cavity of the front projectile at the same time.

The asymmetry of the cavity shape is further enhanced when the lateral flow velocity increases to 11.25%V_p. At t = 1.6 ms, the head of the second projectile is close to the tail of the cavity of the first projectile, which is similar with that at the same time in Figure 17a–c. However, at t = 2.2 ms, the head of the second projectile still did not enter the cavity of the first projectile, and a slight deflection of the trajectory of the second projectile could be observed at this time. At t = 3.4 ms, the trajectory of the second projectile continues to deflect. The second projectile still moves forward in its own cavity, without entering the cavity of the front projectile like that under other conditions. It can be also observed that the cavity size of the first projectile is reduced due to the influence of the second projectile. At this time, the size of the cavity of the second projectile is larger than that of the first one.

Figure 18 shows the change in the axial velocity of the tandem projectiles under different conditions. The horizontal coordinate is the time, and the vertical coordinate is the dimensionless velocity V_x/V_p.
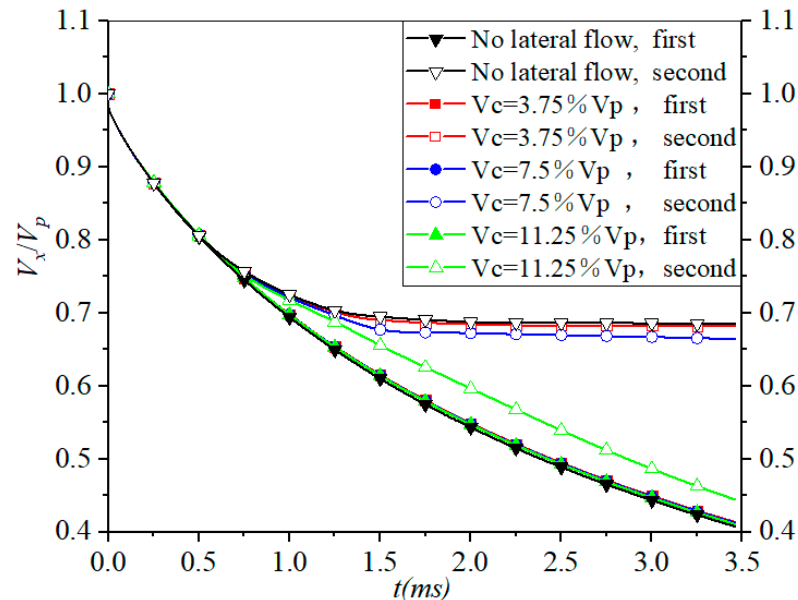

Figure 18. The change in the velocity in the x-direction with the time under different conditions.

It can be seen from the figure that the axial velocity of projectile 1 gradually decreases under all of the conditions. The change in the axial velocity of projectile 2 is somewhat different for different conditions. Under the condition without lateral flow, the change trend is nearly the same as that of projectile 1 before t = 0.75 ms, and after that the change rate of the velocity of projectile 2 becomes slower. After t = 1.75 ms, the velocity of projectile 2 nearly keeps constant. The reason may be due to the fact that the head of projectile 2 at this time has already entered the cavity of the front projectile, and the drag on projectile 2 is

significantly reduced. At t = 3.5 ms, the axial velocity of projectile 1 is reduced by about 60%, while that of projectile 2 is reduced by only about 30%.

Under the condition with the lateral flow velocity of 3.75%V_p, the change in the axial velocity of projectile 2 is nearly the same as that under the condition with no lateral flow. The reason may be as follows: the deformation of the cavity is smaller for this condition, and then the interaction of the cavity of the two projectiles is similar to that under the condition with no lateral flow.

Under the condition with the lateral flow velocity of 7.5%V_p, the axial velocity of projectile 2 decreases slightly faster than that under the condition with the lateral flow velocity of 3.75%V_p near t = 1.5 ms. After t = 1.5 ms, the change in projectile 2 is also nearly unchanged.

Under the condition with the lateral flow velocity of 11.25%V_p, the change trend of the velocity of projectile 2 is similar to that of projectile 1, but the rate of the velocity change in projectile 2 is slightly slower than that of projectile 1. The reason may be that under this condition, projectile 2 does not enter into the cavity of projectile 1 and the two projectiles separately move forward within the cavity of itself. In addition, because projectile 1 moves in front of projectile 2, the fluid behind projectile 1 has a velocity along the x-direction due to the pass of projectile 1, which is helpful to the forward movement of projectile 2. Thus, the reduction in the velocity of projectile 2 is slightly slower than that of projectile 1. At t = 3.5 ms, the reduction in the axial velocity of projectile 1 and 2 is about 60% and 55% of the initial velocity, respectively.

Figure 19 shows the change in the velocity component in the z-direction (named offset velocity) of the tandem projectiles under different conditions. It can be seen from the figure that the offset velocity of the projectiles 1 and 2 is nearly zero under the condition with no lateral flow. That is, both projectiles move forward almost along its initial velocity direction under this condition.
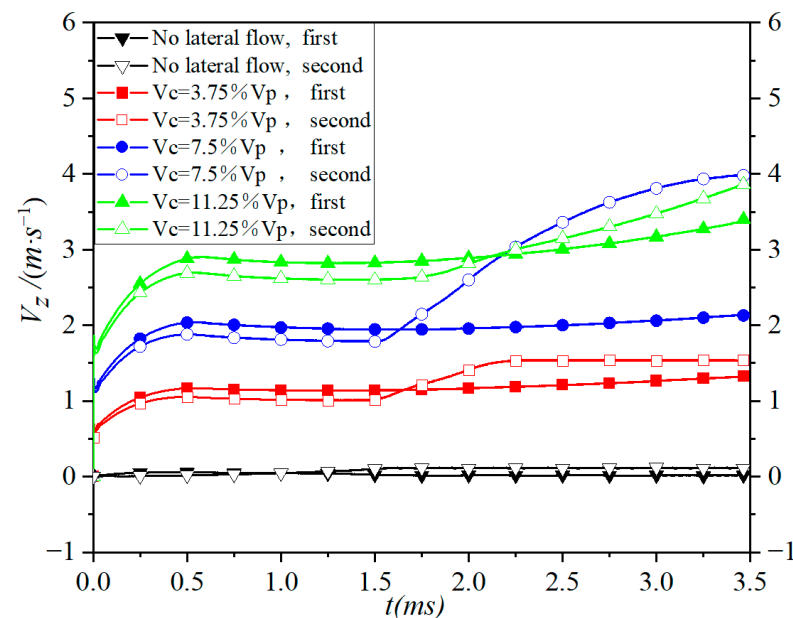

Figure 19. The change in the velocity in the z-direction with the time.

Under the condition with the lateral flow velocity of 3.75%V_p, the offset velocity on the both projectiles is larger than that under the condition with no lateral flow. The offset velocity of the 2 projectiles increases faster before t = 0.5 ms, which is due to the fact that during this period the projectile is not completely wrapped by the cavity and the projectile is more obviously affected by the lateral flow. After t = 0.5 ms, projectile 1 is completely wrapped by the cavity, and the offset velocity of projectile 1 is nearly unchanged. For projectile 2, the offset velocity also remains nearly constant during the period of t = 0.5~1.5 ms.

During this time, projectile 2 is wrapped by its own supercavity like projectile 1. At about t = 1.6 ms, the offset velocity of projectile 2 increases. At this moment, the head of projectile 2 reaches the tail of the cavitation of projectile 1 (Figure 17b). The cavity profile is asymmetric due to the effect of the lateral flow, and there is a locally wetted area near the head of projectile 2. The pressure on projectile 2 is asymmetric and the pressure on the oncoming side of the head of projectile 2 is higher than that on the other parts of the projectile. This results in the increase in the offset velocity of projectile 2. After projectile 2 completely enters the cavity of projectile 1, the offset velocity stays nearly unchanged again.

Under the condition with the lateral flow velocity of 7.5%V_p, the change trend of the offset velocity of the both projectiles is basically the same as that under the condition of the lateral flow velocity of 3.75%V_p. However, the offset velocities of the two projectiles are somewhat increased due to the increase in the lateral flow velocity. In addition, at about t = 1.6 ms, the rate of the increase in the offset velocity of projectile 2 is greater than that under the condition of the lateral flow velocity of 3.75%V_p. This may be due to the increase in the asymmetry of the cavity at this condition. The rewetted area on the oncoming side increases and the lateral force on projectile 2 is increased under this condition. Thus, the offset velocity is increased. At t = 3.5 ms, the offset velocity of projectile 2 reaches about 60% of the lateral flow velocity, while the offset velocity of projectile 1 is only about 30% of that.

Under the condition with the lateral flow velocity of 11.25%V_p, the offset velocities of projectile 1 and projectile 2 are larger than those under other conditions before t = 2.25 ms. For projectile 2, the offset velocity increases at t = 1.6 ms, but the rate of the increase is significantly lower than that under the condition with the lateral flow velocity of 7.5%V_p. The reason is that at this condition projectile 2 does not enter the cavity of projectile 1. At t = 1.6 ms, the increase in the offset velocity of projectile 2 may be not due to the emergence of the rewetted area on the oncoming side of projectile 2, but because of the interaction of the cavity flow field between the two projectiles.

Figure 20a,b shows the change in the deflection angle α and the angular velocity of the projectiles around the y-axis with the time for the tandem projectiles under different conditions, respectively. The positive value in the ordinate indicates that the deflection angle or the angular velocity of the projectile is counterclockwise around the y-axis, and vice versa. It can be seen from the figures that both the deflection angle α and the angular velocity of the two projectiles are nearly zero in the case of no lateral flow. That is, the trajectory of the projectiles is hardly deflected.
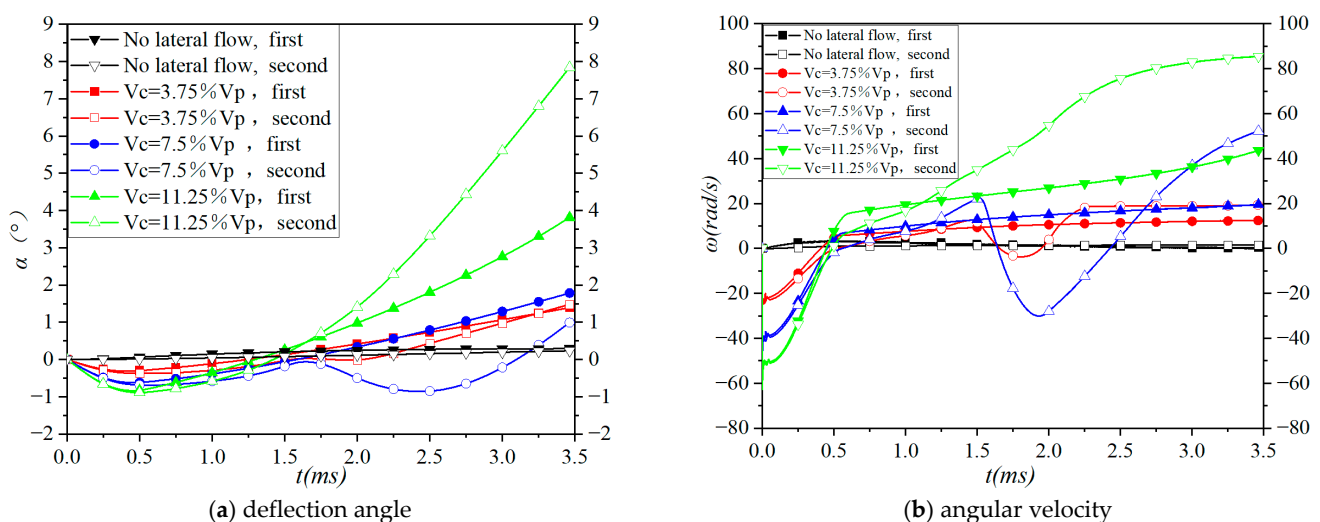

(a) deflection angle   **(b)** angular velocity

Figure 20. Change in the deflection angle α and the angular velocity with the time under different conditions.

For the three conditions with different velocities of the lateral flow, the deflect angle of projectile 1 is firstly clockwise and then counterclockwise. However, for projectile 2 the deflection angle varies among the different conditions.

Under the conditions with the lateral flow velocity of $3.75\%V_p$, the clockwise deflection angle of projectile 2 first increases, then decreases, and finally projectile 2 deflects counterclockwise. During the period of $t = 1.5$ ms~2.25 ms, the gradient of the angular velocity is obviously larger, which can be seen in the change in the deflection angle. The reason of the larger gradient of the angular velocity will be discussed later.

Under the condition with the lateral flow velocity of $7.5\%V_p$, the change trend of both the deflection angle and the angular velocity are similar as those under the condition of the lateral flow velocity with $3.75\%V_p$, but after $t = 1.5$ ms, the change gradient under this condition is more obvious than the condition with $3.75\%V_p$. The reason of the change in the angular velocity after $t = 1.5$ ms can be explained by Figure 21. Figure 21 gives the schematic diagram of the pressure distribution around projectile 2 at two different time points ($t = 1.6$ ms and 2.4 ms).

(**a**) $t = 1.6$ ms, $V_c = 7.5\%V_p$ (**b**) $t = 2.4$ ms, $V_c = 7.5\%V_p$
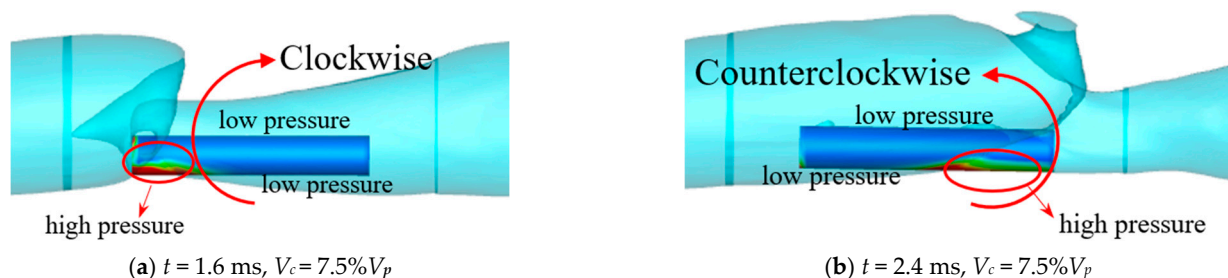
Figure 21. Schematic diagram of the pressure distribution around projectile 2 at two different time points.

In Figure 21a, projectile 2 begins to enter the cavity of the front projectile (at $t = 1.6$ ms). Because of the deformation of the supercavity of the front projectile, a wetted zone on the oncoming side of projectile 2 exists. At the wetted zone, the pressure is higher than that on the other part of projectile 2. The moment and the angular acceleration on projectile 2 at this time is clockwise. Thus, the counterclockwise angular velocity decreases at $t = 1.6$ ms (Figure 20b) due to the clockwise angular acceleration.

In Figure 21b, the tail of projectile 2 is rewetted ($t = 2.4$ ms). The pressure at the rewetted zone (on the coming side of the projectile tail) is higher than that on the other part of the projectile. Thus, the angular acceleration of projectile 2 around the y-axis is counterclockwise at this time. Thus, the angular velocity at $t = 2.4$ ms increases due to the counterclockwise angular acceleration.

For the above 3 conditions with no lateral flow and the lateral flow velocity of $3.75\%V_p$ and $7.5\%V_p$, the deflection angle of the both projectiles is relatively small, which is in the range of $2°$.

Under the condition with the lateral flow velocity of $11.25\%V_p$, the deflection angle is larger than that under other conditions. Both projectile 1 and 2 deflect firstly clockwise and then counterclockwise. At $t = 3.5$ ms, the deflection angle of projectile 1 is about $4°$, while that of projectile 2 is up to $8°$.

5. Conclusions

In this paper, the supercavitation flow field of the parallel and tandem projectiles moving underwater under several conditions was numerically simulated. The effects of the lateral flow on the cavitation evolution, the change in the velocity and the deflection angle of the two projectiles were analyzed. The results of the studies are as follows:

(1)   Under the condition without lateral flow, the shape of the cavity of the parallel projectile group and every tandem projectile is symmetrical. Under the condition with lateral flow, the cavity profile is no longer symmetrical. The size of the cavity on

the oncoming side decreases and that on the backflow side increases. The asymmetry of the cavity contour increases with the velocity of the lateral flow.

(2) For the parallel projectiles, the change trend of the axial velocity of projectile 1 and projectile 2 is nearly the same. The offset velocity of projectile 1 and projectile 2 increases with the increase in the velocity of the lateral flow. Furthermore, the offset velocity of projectile 2 increases obviously with the increase in the velocity of the lateral flow. At $t = 3.0$ ms, under the condition of the lateral flow velocity of $3.75\%V_p$, the offset velocity of projectile 2 is about 33% of the lateral flow velocity, while the offset velocity is up to about 61% of the lateral flow velocity under the condition of the lateral flow velocity of $11.25\%V_p$.

(3) For the tandem projectiles, the change trends of the axial velocity of projectile 1 and projectile 2 are different. The velocity of projectile 1 gradually decreases. The change trend of projectile 2 is different with the different velocity of the lateral flow. Under the conditions of the lateral flow velocities of $3.75\%V_p$ and $7.5\%V_p$, the axial velocity of projectile 2 gradually decreases at first and then stays nearly constant when projectile 2 enters into the cavity of projectile 1. Under the condition of the lateral flow velocity of $11.25\%V_p$, the change trend of the axial velocity of projectile 2 is like that of projectile 1.

(4) For the parallel projectiles, the deflection angle of projectile 1 decreases with the increase in the lateral flow velocity and that of projectile 2 increases with the increase in the lateral flow velocity. At $t = 3.0$ ms, the deflection angle of projectile 2 is up to $20°$ under the condition of the lateral flow velocity of $11.25\%V_p$, while the deflection angles of projectile 1 and projectile 2 under other conditions are in the range of $5°$.

(5) For the tandem projectiles, the deflection angles of the both projectiles are nearly equal to zero under the condition with no lateral flow. Under the conditions with lateral flow, the deflection angle is somewhat complex. The deflection angle demonstrates different changes dependent on the deformation of the cavity, the interaction of the cavity of the two projectiles and the rewetted zone on the projectile wall.

Author Contributions: Methodology, H.J.; software, C.Z.; validation, C.Z.; investigation, C.Z. and H.J.; writing—original draft preparation, C.Z.; writing—review and editing, H.J., L.Z. and R.D.; visualization, C.Z.; supervision, L.Z.; project administration, L.Z.; All authors have read and agreed to the published version of the manuscript.

Data Availability Statement: Not applicable.

References

1. Brennen, C.E. *Cavitation and Bubble Dynamics*; Cambridge University Press: Cambridge, UK, 2013; pp. 110–144.
2. Hirt, C.W.; Nichols, B. Volume of fluid (VOF) method for the dynamics of free boundaries. *J. Comput. Phys.* **1981**, *39*, 201–225. [CrossRef]
3. Ceccio, S.L. Friction Drag Reduction of External Flows with Bubble and Gas Injection. *Annu. Rev. Fluid Mech.* **2010**, *42*, 183–203. [CrossRef]
4. Bimestre, T.A.; Júnior, J.A.M.; Botura, C.A.; Canettieri, E.; Tuna, C.E. Theoretical modeling and experimental validation of hydrodynamic cavitation reactor with a Venturi tube for sugarcane bagasse pretreatment. *Bioresour. Technol.* **2020**, *311*, 123540. [CrossRef] [PubMed]
5. Bimestre, T.A.; Júnior, J.A.M.; Canettieri, E.V.; Tuna, C.E. Hydrodynamic cavitation for lignocellulosic biomass pretreatment: A review of recent developments and future perspectives. *Bioresour. Bioprocess.* **2022**, *9*, 231–239. [CrossRef]

6. Savchenko, Y.N.; Vlasenko, Y.D.; Semenenko, V.N. Experimental Studies of High-Speed Cavitated Flows. *Int. J. Fluid Mech. Res.* **1999**, *26*, 365–374. [CrossRef]
7. Savchenko, Y.N. Modeling the Supercavitation Processes. *Int. J. Fluid Mech. Res.* **2001**, *28*, 16. [CrossRef]
8. Hrubes, J.D. High-speed imaging of supercavitating underwater projectiles. *Exp. Fluids* **2001**, *30*, 57–64. [CrossRef]
9. Vlasenko, Y.D. Experimental Investigation of Supercavitaion Flow Regimes at Subsonic and Transonic Speeds. In Proceedings of the 5th International Symposium on Cavitation, Osaka, Japan, 1–4 November 2003.
10. Nguyen, V.T.; Park, W.G. Numerical study of the thermodynamics and supercavitating flow around an underwater high-speed projectile using a fully compressible multiphase flow model. *Ocean Eng.* **2022**, *257*, 111686. [CrossRef]
11. Shi, H.H.; Takami, T. Hydrodynamic behavior of an underwater moving body after water entry. *Acta Mech. Sinaca (Engl. Ser.)* **2001**, *17*, 35–44.
12. Truscott, T.T.; Techet, A.H. Water entry of spinning spheres. *J. Fluid Mech.* **2009**, *625*, 135–165. [CrossRef]
13. Speirs, N.B.; Mansoor, M.; Belden, J.; Truscott, T.T. Water entry of spheres at various contact Angles. *J. Fluid Mech.* **2019**, *862*, R3. [CrossRef]
14. Li, Q.; Lu, L.; Cai, T. Numerical investigations of trajectory characteristics of a high-speed water-entry projectile. *AIP Adv.* **2020**, *10*, 095107. [CrossRef]
15. Jia, H.X.; Xie, R.S.; Zhou, Y.J. Experimental Investigation of the Supercavitation and Hydrodynamic Characteristics of High-Speed Projectiles with Hydrophobic and Hydrophilic Coatings. *Fluids* **2022**, *7*, 363. [CrossRef]
16. Guo, Z.; Zhang, W.; Xiao, X.; Wei, G.; Ren, P. An investigation into horizontal water entry behaviors of projectiles with different nose shapes. *Int. J. Impact Eng.* **2012**, *49*, 43–60. [CrossRef]
17. Shi, H.H.; Zhou, D.H.; Lu, L.W.; Zhou, D.; Liu, Y. On the water exit of supercavitating projectiles with different head shapes. *Shock Waves* **2021**, *31*, 597–607. [CrossRef]
18. Lu, J.X.; Wang, C.; Song, W.C.; Wei, Y.J.; Yu, D.L.; Li, Y.G. Experimental investigation on interference characteristics of projectiles launched successively underwater. *Ocean Eng.* **2022**, *285*, 110824. [CrossRef]
19. Xu, H.; Wei, Y.J.; Wang, C.; Lu, J.X. On wake vortex encounter of axial-symmetric projectiles launched successively underwater. *Ocean Eng.* **2019**, *189*, 106382. [CrossRef]
20. Lu, L.; Yan, X.; Li, Q.; Wang, C.; Shen, K.C. Numerical study on the water-entry of asynchronous parallel projectiles at a high vertical entry speed. *Ocean Eng.* **2022**, *250*, 111026. [CrossRef]
21. Qi, C.; Wang, X.; Lyu, X.J. On the flow characteristics of two supercavitating projectiles moving in water side-by-side. *Phys. Fluids* **2022**, *35*, 017127. [CrossRef]
22. Zhou, D.H.; Shi, H.H.; Jia, H.X. Characteristics of the multiphase flow field with super-cavitation induced by successively fired projectiles under-water and cross-medium. *J. Mech. Sci. Technol.* **2022**, *36*, 247–258. [CrossRef]
23. Yu, D.L.; Wang, C.; He, C.J. Numerical simulation of cavitation and motion characteristics of revolution bodies entering water in parallel. *J. Harbin Inst. Technol.* **2021**, *53*, 23–32. (In Chinese)
24. Wang, M.; Fan, C.Y.; Hou, G.S. Numerical research of lateral flow influence on supercavitating flow. *AIP Adv.* **2022**, *12*, 045214. [CrossRef]
25. Zhou, L.; Wang, Z. Numerical Simulation of Cavitation Around a Hydrofoil and Evaluation of a RNG κ-ε Model. *J. Fluids Eng. -Trans. Asme* **2008**, *130*, 011302. [CrossRef]
26. Schnerr, G.H.; Sauer, J. Physical and numerical modeling of unsteady cavitation dynamics. In Proceedings of the Fourth International Conference on Multiphase Flow (ICMF), New Orleans, LO, USA, 27 May–1 June 2001; Volume 1.
27. Watanabe, R.; Fujii, K.; Higashiura, F. Computational analysis of the unsteady flow induced by a projectile overtaking a preceding shock wave. *Trans. Jpn. Soc. Aeronaut. Space Sci.* **1998**, *41*, 65–73.